Tsunami early warning using earthquake rupture duration and *P*-wave dominant-period: the importance of length and depth of faulting

Anthony Lomax[1] and Alberto Michelini[2]

[1]ALomax Scientific, Mouans-Sartoux, France. E-mail: anthony@alomax.net

[2]Istituto Nazionale di Geofisica e Vulcanologia, Roma, Italy

Accepted for publication in Geophysical Journal International

Accepted 2010 December 06. Received 2010 December 06; in original form 2010 April 02.

After an earthquake, rapid, real-time assessment of hazards such as ground shaking and tsunami potential is important for early warning and emergency response. Tsunami potential depends on sea floor displacement, which is related to the length, *L*, width, *W*, mean slip, *D*, and depth, *z*, of earthquake rupture. Currently, the primary discriminant for tsunami potential is the centroid-moment tensor magnitude, M_w^{CMT}, representing the seismic potency *LWD*, and estimated through an indirect, inversion procedure. The obtained M_w^{CMT} and the implied *LWD* value vary with the depth of faulting, assumed earth model and other factors, and is only available 30 min or more after an earthquake. The use of more direct procedures for hazard assessment, when available, could avoid these problems and aid in effective early warning. Here we present a direct procedure for rapid assessment of earthquake tsunami potential using two, simple measures on *P*-wave seismograms – the dominant period on the velocity records, T_d, and the likelihood that the high-frequency, apparent rupture-duration, T_0, exceeds 50-55 sec. T_0 can be related to the critical parameters *L* and *z*, while T_d may be related to *W*, *D* or *z*. For a set of recent, large earthquakes, we show that the period-duration product T_dT_0 gives more information on tsunami impact and size than M_w^{CMT} and other currently used discriminants. All discriminants have difficulty in assessing the tsunami potential for oceanic strike-slip and back-arc or upper-plate, intraplate earthquake types. Our analysis and results suggest that tsunami potential is not directly related to the potency *LWD* from the "seismic" faulting model, as is assumed with the use of the M_w^{CMT} discriminant. Instead, knowledge of rupture length, *L*, and depth, *z*, alone can constrain well the tsunami potential of an earthquake, with explicit determination of fault width, *W*, and slip, *D*, being of secondary importance. With available real-time seismogram data, rapid calculation of the direct, period-duration discriminant can be completed within 6-10 min after an earthquake occurs and thus can aid in effective and reliable tsunami early warning.

Introduction

After an earthquake, rapid, real-time assessment of hazards such as ground shaking and tsunami potential is important for early warning and emergency response (e.g., Kanamori 2005; Bernard *et al*. 2006). Effective tsunami early warning for coastlines at regional distances (>100 km) from a tsunamigenic earthquake requires notification within 15 minutes after the earthquake origin time (OT). Currently, rapid assessment of the tsunami potential of an earthquake by organizations such as the Japan Meteorological Agency (JMA), the German-Indonesian tsunami early warning system (GITEWS) or the West Coast and Alaska (WCATWC) and Pacific (PTWC) Tsunami Warning Centers relies mainly on initial estimates of the earthquake location, depth and moment, M_0, or the corresponding moment magnitude, M_w. For the regional scale, WCATWC and PTWC issue warning notifications within about 5-10 min after OT for shallow, underwater events using the *P*-wave moment-magnitude discriminant, M_{wp}, (Tsuboi *et al*. 1995; Tsuboi *et al*. 1999) if $M_{wp} \geq 7.5$ (e.g., Hirshorn *et al*. 2009).

M_0 is of interest for tsunami warning because the efficiency of tsunami generation by a shallow earthquake is dependent on the amount of sea floor displacement, which can be related to a finite-faulting model expressed by the seismic potency, *LWD*, where *L* is the length, *W* the width and *D* the mean slip of the earthquake rupture (e.g., Kanamori 1972; Abe 1973; Kajiura 1981; Lay and Bilek 2007; Polet and Kanamori 2009). Then, since $M_0 = \mu LWD$, where μ is the shear modulus at the source, the sea-floor displacement and thus tsunami potential should scale with $LWD = M_0/\mu$. If μ is taken as constant for all shallow earthquakes, M_0 and the corresponding M_w should be good discriminants for tsunami potential; indeed, for a point source, the tsunami wave amplitude is expected to be directly proportional to M_0 (Okal 1988).

M_w is found to be a good discriminant for many, past, tsunamigenic earthquakes, but not all, especially not for so-called "tsunami earthquakes", which, by definition, cause larger tsunami waves than would be expected from their M_w (e.g., Kanamori 1972; Satake 2002; Polet and Kanamori 2009). The discrepancy for these earthquakes can be related to rupture at shallow depth where μ can be very low, an-elastic deformation such as ploughing and uplift of sediments may occur, and the fault surface may be non-planar with splay faulting into the accretionary wedge (e.g., Fukao 1977; Moore *et al*. 2007; Lay and Bilek 2007). One or more of these effects can result in an underestimate by M_0 or M_w of an effective *LWD* value by a factor of 4 or more relative to the value needed to explain the observed tsunami waves (Okal 1988; Satake 1994; Geist and Bilek 2001; Lay and Bilek 2007; Polet and Kanamori 2009).

The assessment of tsunami potential using M_0 follows an indirect procedure: firstly, an earthquake source model (e.g., hypocenter, M_0) is determined from basic observations using a physical theory, earth model and an inversion algorithm, and, secondly, the critical parameters (e.g., *LWD*) that estimate the hazard are (explicitly or implicitly) extracted from this source model. This procedure involve assumptions and algorithms that introduce error and sometimes large processing-time delays. For M_0, as noted above, an error in source depth or use of an inappropriate earth model can lead to error in the estimated *LWD*, while obtaining M_0 requires inversion of long period seismic waves which introduces a delay of 30 min or more after OT. The use of direct and rapid procedures to constrain critical parameters such as *L*, *W* and *D* and assess tsunami potential could avoid these problems and, in some cases, make possible effective tsunami early warning for coastlines near a tsunamigenic earthquake. Direct procedures are currently used to estimate magnitudes and shaking intensity for earthquake early warning and rapid response (e.g., Wald *et al.* 1999; Kanamori 2005; Lancieri and Zollo 2008).

Recently, through analysis of teleseismic, *P*-wave seismograms (30°-90° great-circle distance; GCD), Lomax and Michelini (2009A; LM2009A hereinafter) have shown that a high frequency, apparent rupture-duration, T_0, greater than about 50 s forms a reliable discriminant for tsunamigenic earthquakes (Fig. 1). Lomax and Michelini (2009B; LM2009B hereinafter) exploit this result through a direct, "duration-exceedance" (DE) procedure applied to seismograms at 10-30° GCD to rapidly determine if T_0 for an earthquake is likely to exceed 50-55 s and thus to be a potentially tsunamigenic earthquake.

Here we present a direct procedure for assessing tsunami potential which combines T_0 with a measure of the dominant period on the velocity records, T_d. T_d and T_0 are simple to measure on observed, *P*-wave seismograms and can be related to the critical parameters *L, W*, *D* and depth needed for assessing tsunami potential. This direct, period-duration procedure gives improved identification of recent earthquakes which produced large or devastating tsunamis, relative to the use of the M_w, teleseismic T_0 or DE discriminants.

Tsunami size, moment magnitude and rupture duration

We consider a reference set of 117 large earthquakes ($6.4 \geq M_w \geq 9.0$; 101 shallow, under water) since 1992, when high-quality, broadband seismograms became widely available, along with the impact and size of any generated tsunamis (Table S1). This reference set includes most tsunamigenic earthquakes listed in the NOAA/WDC Historical Tsunami Database (http://www.ngdc.noaa.gov/hazard/tsu_db.shtml), most events of $M_w \geq 7$ in the past few years and several events of regional importance.

Lacking a uniform, physical measure of impact for most tsunamis, following *LM2009A,B*, we define a approximate measure of tsunami importance, I_t, for the reference earthquakes based on 0-4 descriptive indices, i_{effect}, of tsunami effects (deaths, injuries, damage, houses destroyed), and maximum water height h in meters from the NOAA/WDC database: $I_t = i_{height} + i_{deaths} + i_{injuries} + i_{damage} + i_{houses\text{-}destroyed}$, where i_{height}=4,3,2,1,0 for $h \geq 10$, 3, 0.5 m, $h > 0$ m, $h = 0$ m respectively. We ignore earthquakes not in the database if they are aftershocks of large events, otherwise we set $I_t = 0$. Note that I_t is approximate since it depends strongly on the available instrumentation, coastal bathymetry and population density in the event region. $I_t \geq 2$ corresponds approximately to the JMA threshold for issuing a "Tsunami Warning"; the largest or most devastating tsunamis typically have $I_t \geq 10$.

For a measure of tsunami size, we calculate a representative tsunami wave amplitude at 100km distance from the source, A_t, for each event, using the water height readings in the NOAA/WDC database corrected to zero to peak, deep-water amplitudes, h_i, and to a distance of 100km using the conservation of energy on the wave front on a spherical surface (e.g., *Woods and Okal* 1987), $a_i = h_i \sin^{1/2}(\Delta)/\sin^{1/2}(\Delta_{100})$, where Δ and Δ_{100} are the angular distances of the height measure from the source and corresponding to 100km, respectively. A_t is the median of the a_i, calculated for events with 3 or more water height readings.

As discriminants for tsunami potential, we first consider the Global Centroid-Moment Tensor moment-magnitude, M_w^{CMT} (Dziewonski *et al.* 1981; Ekström *et al.* 2005), and T_0 durations calculated from the envelope decay of squared, high-frequency (HF; 1-5 Hz band-pass), P-wave seismograms at teleseismic distance (LM2009A). Fig. 2 shows M_{wp}, M_w^{CMT} and T_0 compared with the impact and size measures I_t and A_t. The thresholds $M_w^{CMT} \geq 7.5$ and $T_0 \geq 55$ s (despite a relatively high uncertainty for the T_0 values) both identify most of the events with $I_t \geq 2$ (see also Tables 1 and S1). However, unlike T_0, M_w^{CMT} shows no clear relationship to I_t or A_t; this difference is especially marked for tsunami earthquakes (type T) and back-arc intraplate events (type B). Relative to a possible linear relationship between A_t and M_0 (Fig. 2, lower centre), M_w^{CMT} is too high for some events, and too low for others, notably for T and some B type events. In contrast, T_0 tends to increase for events with larger I_t and A_t, including for types T and B, and shows possible agreement with a linear relationship between between A_t and T_0 (Fig. 2, lower right).

Faulting dimensions, rupture duration and dominant period

The M_0 (or M_w^{CMT}) discriminant relies on the assumption that tsunami potential is directly related to the *LWD* or potency, finite-faulting description of the source, while the shortcomings of this discriminant for tsunami and other earthquakes are in part related to depth of rupture. Rupture duration, T_0, corresponds well to the tsunami size measures I_t and A_t because T_0 is related to a component of the *LWD* source, the rupture length L: $T_0 \propto L/v_r$, where v_r is rupture velocity. Since v_r scales with *S*-wave velocity and shear modulus, μ, which increase with depth, and since v_r is found to be very low at shallow depth for tsunami earthquakes (Geist and Bilek 2001; Polet and Kanamori 2009), we may assume $v_r \propto z^q$, where z is some mean rupture depth (e.g., Kajiura 1981) and q is positive. Then, $T_0 \propto L/z^q$, showing that T_0 provides information on both L and z, and, most importantly, T_0 grows with increasing L and decreasing z, two conditions for increased tsunami potential.

The above considerations suggest a general relation for *tsunami potential* involving L, W, D and the mean rupture depth, z, of the form LWD/z^p, with p positive. Such a relationship could be evaluated by combining T_0, which gives information on L and z, with additional information on W, D and z.

Information on W, D and z may be provided by the frequency content of the *P*-wave seismogram. For example, consider the corner frequency of the *P*-wave displacement spectrum, f_c. The corresponding period, $1/f_c$, can be related to a linear dimension of the earthquake rupture, typically $\sqrt{A}$, where A is the rupture area (e.g., Brune 1970; Madariaga 1976; Madariaga 2009). However, since we consider here large earthquakes with $L>W$ or $L>>W$, $1/f_c$ is more likely related to W than to L, e.g. $W \propto v_r/f_c$. For the fault displacement, D, there is controversy whether $D \propto W$ or $D \propto L$ for large crustal earthquakes, but for subduction zone, thrust events that concern us most, W may grow with L (Scholz 1982), which allows $D \propto W$ and thus the possibility that $D \propto v_r/f_c$. In addition, tsunami earthquakes and shallow, near trench earthquakes are characterised by a deficiency in high-frequency radiation (e.g., Shapiro et al., 1998; Polet and Kanamori 2000; Polet and Kanamori 2009). Thus a characterisation of the frequency content of the *P*-wave seismograms may provide information on W, D and z, with anomalously low frequencies indicating increased W or D, or decreased z, and correspondingly increased tsunami potential.

Here we choose to characterise the *P*-wave frequency content by its dominant-period, obtained by applying the rapid, time-domain, τ_c algorithm (Nakamura 1988; Wu and Kanamori 2005) to velocity seismograms. Given a *P*-wave velocity seismograms, $v(t)$, τ_c, is given by,

$$\tau_c = 2\pi \sqrt{\int_{T_1}^{T_2} v^2(t)\,dt \Big/ \int_{T_1}^{T_2} \dot{v}^2(t)\,dt} \quad , \tag{1}$$

with the integrals taken over the time window (T_1, T_2).

We define the dominant period, t_d, as the peak τ_c value obtained from eq.(1) applied with a 5 s sliding time-window from 0 to 55 s after the *P* arrival. This definition of t_d follows from examination of numerous possible parameter settings with the goal of best discriminating tsunamigenic events. The value of 5 s for the time-window is sufficient to identify if t_d is greater or less than about 10 s, which we will see below is roughly the critical value for discrimination using t_d along with T_0. We use *P*-wave seismograms only within the distance range of 5-40° GCD to avoid biases due to distance- and frequency-dependent attenuation, ignored here due to lack of accurate attenuation models for the earthquake source regions. Where the signal is predominantly monochromatic, the obtained t_d values match well the dominant period of *P*-waves found by visual inspection of seismograms (Fig. 1).

We define an event T_d level as the median of the station t_d values, with station distribution weighting applied to balance the contribution of sometimes highly heterogeneously distributed (e.g. clustered or isolated) stations. Fig. 3 shows a comparison of event T_d (median of the station t_d values) with I_t and A_t - there is an overall increase in T_d with respect to increasing I_t, though much scatter, and an unclear but possibly similar relation between T_d and A_t.

To investigate relationships of the form LWD/z^p for determining tsunami potential we have examined numerous expressions such as $T_d^2 T_0$, $T_d T_0^2$ and $T_d T_0$ as discriminants and found that $T_d T_0$ gives the best agreement with I_t and A_t. Fig. 3 shows a comparison of $T_d T_0$ with I_t and A_t.

The discriminant T_dT_0 (despite a relatively large uncertainty; see Table S1) has a clearer correspondence to I_t and A_t than M_w^{CMT} and T_0 (Fig. 2), including for tsunami earthquakes (type T) and some back-arc intraplate earthquakes (type B). The main contribution to this correspondence comes from the T_0 values, while the T_d values, despite their scatter, help to improve the results for larger events and those with I_t=0. T_dT_0 also shows possible agreement, as good or better than that of T_0, to a linear relationship with A_t (Fig. 3, lower centre). A critical threshold value of T_dT_0 = 510 s^2 shows improved identification of events with $I_t \geq 2$ and of non-tsunamigenic events with I_t=0 relative to M_w^{CMT} and T_0 (Figs. 2 and 3; Table 1). This result indicates a critical value for T_d of about 10 s, since the critical threshold for the T_0 discriminant alone is 55 s.

Rapid, direct assessment of tsunami potential

Since moment-based magnitudes such as M_w^{CMT} are only available 30 min or later after OT, rapid magnitude estimates such as M_{wp} are used for tsunami warning. But M_{wp} performs poorly relative to M_w^{CMT}, T_0 or T_dT_0 for identifying events with $I_t \geq 2$ (Fig. 2; Table 1). Other rapid magnitude estimates for large earthquakes (e.g., Hara 2007; M_{wpd}, *LM2009A*; m_{Bc}, Bormann and Saul 2009; M_{ww}, Kanamori and Rivera *20*08) may perform nearly as well as M_w^{CMT} or T_0 (e.g., M_{wpd} in Tables 1 and S1), but are not available until about 15 min or later after OT.

Rapid, real-time determination if T_dT_0 exceeds a critical threshold (i.e., $T_dT_0 \geq 510$ s^2) would provide important complementary information to initial location, depth and magnitude estimates for early assessment of earthquake tsunami potential. Since T_d is obtained rapidly (<60 s) after the *P* arrival, it remains to rapidly asses T_0 for an earthquake, in particular if $T_0 \geq$50-55 s. Using the duration-exceedance, DE, procedure of *LM2009B*, we determine if T_0 for an earthquake is likely to exceed 50-55s through HF analysis of vertical-component, broadband seismograms. On 1-5 Hz band-pass filtered seismogram we form the ratio of the *rms* amplitude from 50-60 s after the *P* with the *rms* amplitude for the first 25 s after the *P* to obtain a station DE level for 50-55 s, l_{50} (Fig. 1). We define an event DE level, L_{50}, as the median of the station l_{50} values, with station distribution weighting and ignoring stations at less than 10° GCD to avoid noisy, anomalously long, and *S*-wave HF signal. If an event DE level L_{50} is greater (less) than 1.0, then T_0 is likely (unlikely) to exceed 50-55 s. Based on this study and our previous work (LM2009A,B) with large earthquakes datasets, we estimate that measures from 10-20 stations are needed to obtain stable estimates of T_0, L_{50} and T_d.

Using L_{50} as a substitute for T_0, our discriminant for tsunami potential becomes T_dL_{50} (i.e., $T_dL_{50} \geq 8.0$ s). We apply the T_dL_{50} discriminant to the reference earthquakes using data up to 10 min after OT from stations up to 30° GCD from each event to simulate the information available in the first minutes after an earthquake occurs. Fig. 3 shows a comparison of T_dL_{50} with I_t and A_t, the overall T_dL_{50} results are listed in Table 1 and all event parameters and results listed in Table S1. A comparison of the T_dL_{50} and T_dT_0 discriminants shows similar performance for identifying events with $I_t \geq 2$ and I_t<2, confirming that the rapidly available T_dL_{50} measures form reliable proxies for T_dT_0 using the teleseismic, T_0 durations.

Discussion

The period-duration discriminants T_dT_0 and T_dL_{50} correctly identify 77% of tsunamigenic events with $I_t \geq 2$, more than the M_w^{CMT} and T_0 discriminants, with fewer false positive identifications of events with I_t<2 (Tables 1 and S1; Figs. 2 and 3). The T_dT_0 and T_dL_{50} discriminants miss 11 tsunamigenic events, all are also missed using the M_w^{CMT} discriminant, except for one, an oceanic, strike-slip earthquake, I_t=6, M_w7.5, 2000.05.04 Sulawesi missed by T_dL_{50}. The events missed by T_dT_0 and T_dL_{50} with largest I_t include two oceanic, strike-slip events, I_t=13, M_w7.1, 1994.11.14 Philippines and I_t=8, M_w6.7, 2006.03.14 Seram Indonesia, a shallow, offshore thrust event, I_t=8, M_w6.8, 2003.05.21 N Algeria, and a back-arc interplate event, I_t=9, M_w6.9, 1995.05.14 Timor associated with a landslide-induced tsunami (NOAA/WDC database). There are 7 events for T_dT_0 and 11 for T_dL_{50} that are falsely identified as likely tsunamigenic, most of these have I_t=1 and thus produced small tsunamis.

Real-time calculation of the rapid discriminant T_dL_{50} does not require accurate knowledge of the earthquake location or magnitude and, for most events, stable L_{50} (LM2009B) and T_d values are available within 6-10 min after OT. The overall performance of the T_dL_{50} discriminant is marginally better than M_w^{CMT}, M_{wpd}, and teleseismic T_0 (Table 1), though these latter three measures are not available until at least 30, 15 and 15 min, respectively, after OT (LM2009A). In contrast, the rapidly available M_{wp} discriminant correctly identifies only 52% of tsunamigenic events with $I_t \geq 2$ (Fig. 2; Table 1), primarily because M_{wp} underestimates the size of events with M_w^{CMT}>7.0-7.5, particularly tsunami earthquakes and other events with long rupture duration (e.g., LM2009A). The T_dL_{50} discriminant also outperforms the energy-to-moment parameter, Θ, useful for identification of tsunami earthquakes (Newman and Okal 1998), because Θ is not a good indicator for tsunamigenic events in general (LM2009A).

Like M_w^{CMT} and T_0, the period-duration discriminants gives mixed results for identifying the tsunami potential of oceanic, strike-slip events (Type *So*). Some of these events may be falsely identified as tsunamigenic (i.e., if they have high magnitude or T_0) since the tsunami excitation for a vertical, strike-slip fault is very low relative to other faulting types (e.g. Kajiura 1981). In contrast, other oceanic, strike-slip events may be missed as tsunamigenic (i.e., if they have moderate magnitude or T_0) because their tsunamis excitation can be augmented by horizontal displacement of ocean floor topography (Tanioka and Satake 1996), an effect which is somewhat independent of source size *LWD* and thus not well quantified by any of the M_w^{CMT}, T_0 or T_dT_0 discriminants.

The T_dT_0 discriminant identifies better than M_w^{CMT} and T_0 some of the tsunamigenic, back-arc intraplate earthquakes (Type B). However, the T_0, T_d and T_dT_0 values for this event type are generally lower than for other event types with similar tsunamigenic impact, suggesting that characteristics other than fault length, width or slip affect the tsunami potential for some back-arc intraplate events. For example, some of these events may involve rupture on steeply dipping faults, which could augment the tsunamigenic strength of these events (e.g., Kajiura 1982), though fault dip is probably not reflected directly in either the M_w^{CMT} or T_dT_0 discriminants.

The improved correspondence to I_t and A_t of the period-duration discriminants relative to M_w^{CMT} and T_0, and the sensitivity of these discriminants to specific source types (e.g. *T*, *P*, *So*; Figs. 2 and 3; Table S1) lend support to the *L*, *W*, *D* and *z* scaling arguments used here. It may be that the T_dT_0 discriminant inherently avoids underestimate of tsunami potential due to incorrect source depth or earth model, as can occur with the indirect, M_0 inversion procedure and corresponding M_w discriminants. Effectively, as shown schematically in Fig. 4, for a fault of fixed potency *LWD*, as rupture depth decreases the rupture velocity, v_r, also decreases, so T_0 and T_d, when interpreted as related to L/v_r, W/v_r or D/v_r, must increase. Thus the quantity T_dT_0 increases with decreasing rupture depth, more or less correctly reflecting the increased tsunami potential of the shallowest, underwater earthquakes, including tsunami earthquakes. This behaviour suggests that the T_dT_0 discriminant captures the "tsunami" faulting model reflecting the observed tsunami waves (Satake 1994), as opposed to the "seismic" faulting model as given by M_0. In this case T_dT_0 may also be a valuable aid in defining the finite-faulting description of the source and sea floor displacement for real-time tsunami forecasting.

From the preceding, we can identify the most critical parameters for discrimination of earthquake tsunami potential. The performance of the T_dT_0 discriminant, though improved by the T_d values, is dominated by the T_0 values (e.g., Figs. 2 and 3), and T_0 for large earthquakes is probably related primarily to rupture length, L. Additionally, we have shown that T_0, T_d and T_dT_0 may inherently account for source depth, and that T_dT_0 may be proportional to A_t. These results imply that knowledge of rupture length, L, and depth, z, alone can constrain well the tsunami potential of an earthquake. Then information on the fault width, W, and slip, D is of secondary importance, though perhaps provided by T_d for some event types, or implicitly through scaling relations such as $W \propto L$ and $D \propto L$. In this case, and considering the poor match of M_w^{CMT} to a linear relation between A_t and M_0 (Fig. 2), there is the suggestion that tsunami potential is not a simple function of the potency LWD from the "seismic" faulting model, as is assumed with the use of the M_w^{CMT} discriminant.

Conclusions

The period-duration discriminant, T_dT_0, for tsunami potential of an earthquake makes use of two direct, P-wave measures: dominant period, T_d, on velocity records and HF, apparent rupture duration, T_0. We have shown empirically that the T_dT_0 discriminant, perhaps through characterisation of a quasi finite-faulting description of the source and of the source depth, provides more information on tsunami importance, I_t, and tsunami amplitude, A_t, than do other discriminants, including teleseismic T_0 alone and centroid-moment tensor magnitude, M_w^{CMT}. The T_dT_0 discriminant correctly identifies 77% of tsunamigenic events ($I_t \geq 2$) in our dataset, while teleseismic T_0 and M_w^{CMT} each identify 68% (Table 1). The value of the T_dT_0 discriminant has relatively large uncertainty, but avoids the possible processing-time delay and error, including underestimate of tsunami potential for shallow earthquakes, of indirect, moment-tensor determinations. Additional improvement in the T_dT_0 discriminant may follow from further development of the T_d algorithm or investigation of other procedures for rapidly extracting information on the frequency content of P waveforms. And the possibility of a linear relationships between A_t and T_dT_0 (Fig. 3) suggests that T_dT_0 or related measures may ultimately prove useful for rapid, quantitative estimates of tsunami wave heights.

Our analysis and the likely, inherent sensitivity of T_dT_0 to rupture length and source depth, indicate that the tsunami potential for most earthquake types can be well constrained by knowledge of the rupture length, L, and some mean rupture depth, z, while explicit information on the fault width, W, or slip, D, is of lessor importance. Moreover, the results imply that tsunami potential is not a simple function of the potency LWD as is assumed with the use of the M_w^{CMT} discriminant. The tsunami potential for many oceanic strike-slip, and back-arc intraplate earthquakes types, however, is not well constrained by any of the discriminants analysed here; further study is warranted to find direct measures and discriminants for these event types, which are occasionally highly tsunamigenic.

For rapid estimation of T_dT_0, the discriminant T_dL_{50} combines T_d with the likelihood that T_0 exceeds 50-55 s. The T_dL_{50} assessment can be completed within 6-10 min after OT for most regions using currently available, real-time seismograms and should form a valuable complement to initial estimates of the location, depth and magnitude of an earthquake to improve the reliability of or make possible tsunami early warning.

Acknowledgements

We thank two anonymous reviewers for helpful comments. This work is supported by the 2007-2009 Dipartimento della Protezione Civile S3 project. We use SeisGram2K (http://www.alomax.net/software) for seismogram analysis and figures, and OpenOffice.org for spreadsheet calculations, graphs and figures. The IRIS DMC (http://www.iris.edu) provided access to waveforms used in this study; we thank all those who install, operate and maintain seismic stations worldwide.

References

Abe, K., 1973. Tsunami and mechanism of great earthquakes, *Phys. Earth Planet. Int.*, *7*, 143-153.

Bernard, E.N., H.O Mofjeld, V. Titov, C.E Synolakis and F.I González, 2006. Tsunami: scientific frontiers, mitigation, forecasting and policy implications, *Phil. Trans. R. Soc. A*, 1989-2007, doi:10.1098/rsta.2006.1809

Brune, J. N., 1970. Tectonic Stress and the Spectra of Seismic Shear Waves from Earthquakes, *J. Geophys. Res.*, *75*, 4997-5009, doi:10.1029/JB075i026p04997

Bormann, P. & Saul, J., 2009. Earthquake magnitude, in *Encyclopedia of Complexity and Systems Science*, edited by A. Meyers, Springer, New York, 10370pp., doi:10.1007/978-0-387-30440-3_151

Dziewonski, A., T.A. Chou, and J. H. Woodhouse, 1981. Determination of earthquake source parameters from waveform data for studies of global and regional seismicity, *J. Geophys. Res.*, *86*, 2825-2852.

Ekström, G., A. M. Dziewonski, N. N. Maternovskaya, and M. Nettles, 2005. Global seismicity of 2003: Centroid-moment-tensor solutions for 1087 earthquakes, *Phys. Earth Planet. Inter.*, *148*, 327– 351.

Fukao, Y., 1979. Tsunami Earthquakes and Subduction Processes Near Deep - Sea Trenches, *J. Geophys. Res.*, *84*, 2303-2314.

Geist, E. L., and S. L. Bilek,, 2001. Effect of depth - dependent shear modulus on tsunami generation along subduction zones, *Geophys. Res. Lett.*, *28*, 1315-1318, doi:10.1029/2000GL012385

Hara, T., 2007. Measurement of the duration of high-frequency energy radiation and its application to determination of the magnitudes of large shallow earthquakes, *Earth Planets Space*, *59*, 227–231.

Hirshorn, B., and S. Weinstein, 2009. Rapid estimates of earthquake source parameters for tsunami warning, in *Encyclopedia of Complexity and Systems Science*, edited by A. Meyers, Springer, New York, 10370pp., doi:10.1007/978-0-387-30440-3_160

Hirshorn, B., S. Weinstein, 2009. Rapid Estimates of Earthquake Source Parameters for Tsunami Warning (ed. A. Meyers), Springer, New York, .

Kanamori, H., 1972. Mechanism of tsunami earthquakes, *Phys. Earth Planet. Int.*, 6, 246 - 259.

Kanamori H., 2005. Real-time seismology and earthquake damage mitigation. *Annu. Rev. Earth Planet. Sci*, *33*, 195–214.

Kanamori, H. and L. Rivera, 2008. Source inversion of W phase: speeding up seismic tsunami warning, *Geophys. J. Int.*, *175*, 222-238, doi: 10.1111/j.1365-246X.2008.03887.x

Kajiura, K., 1981. Tsunami energy in relation to parameters of the earthquake fault model, *Bulletin of the Earthquake Research Institute*, *56*, 415–440.

Lancieri, M. and A. Zollo, 2008. A Bayesian approach to the real - time estimation of magnitude from the early and wave displacement peaks, *J. Geophys. Res.*, *113*, B12302, doi:10.1029/2007JB005386.

Lay, T., and S. Bilek, 2007. Anomalous earthquake ruptures at shallow depths on subduction zone megathrusts, in *The Seismogenic Zone of Subduction Thrust Faults*, edited by T. H. Dixon and C. Moore, Columbia Univ. Press, New York, 692pp, ISBN: 978-0-231-13866-6.

Lomax, A., 2005. Rapid estimation of rupture extent for large earthquakes: application to the 2004, M9 Sumatra-Andaman mega-thrust, *Geophys. Res. Lett.*, *32*, L10314, doi:10.1029/2005GL022437

Lomax, A. and A. Michelini, 2005. Rapid Determination of Earthquake Size for Hazard Warning, *Eos Trans. AGU*, *86*(21), 202.

Lomax, A., A. Michelini and A. Piatanesi, 2007. An energy-duration procedure for rapid determination of earthquake magnitude and tsunamigenic potential, *Geophys. J. Int.*, *170*, 1195-1209, doi:10.1111/j.1365-246X.2007.03469.x

Lomax, A. and A. Michelini, 2009A. M_{wpd}: A duration-amplitude procedure for rapid determination of earthquake magnitude and tsunamigenic potential from *P* waveforms, *Geophys. J. Int.*, *176*, 200–214, doi:10.1111/j.1365-246X.2008.03974.x

Lomax, A. and A. Michelini, 2009B. Tsunami early warning using earthquake rupture duration, *Geophys. Res. Lett.*, *36*, L09306, doi:10.1029/2009GL037223

Madariaga, R., 1976. Dynamics of an expanding circular fault, *Bull. Seism. Soc. Am.*, *66*, 639-666.

Madariaga, R., 2009. Earthquake Scaling Laws, in *Encyclopedia of Complexity and Systems Science*, edited by A. Meyers, Springer, New York, 10370pp., doi:10.1007/978-0-387-30440-3_156

Moore, G. F., N. L. Bangs, A. Taira, S. Kuramoto, E. Pangborn, H. J. Tobin, 2007. Three-Dimensional Splay Fault Geometry and Implications for Tsunami Generation. *Science* 318, 1128, DOI: 10.1126/science.1147195

Nakamura, Y., 1988. On the urgent earthquake detection and alarm system (UrEDAS), *Proc. of the 9th World Conference on Earthquake Engineering*, Tokyo-Kyoto, Japan.

Newman, A.V., and E.A. Okal, 1998. Teleseismic Estimates of Radiated Seismic Energy: The E/M_0 Discriminant for Tsunami Earthquakes, *J. Geophys. Res.*, *103*, 26,885-26,898.

Okal, E.A., 1988. Seismic parameters controlling far-field tsunami amplitudes: a review, *Natural Hazards*, *1*, 67–96.

Polet, J., and Kanamori, H., 2000. Shallow subduction zone earthquakes and their tsunamigenic potential. *Geophys. J. Int.*, *142*, 684–702.

Polet, J., and H. Kanamori, 2009. Tsunami Earthquakes, in *Encyclopedia of Complexity and Systems Science*, edited by A. Meyers, Springer, New York, 10370pp., doi:10.1007/978-0-387-30440-3_567

Satake, K., 1994. Mechanism of the 1992 Nicaragua Tsunami Earthquake, *Geophys. Res. Lett.*, *21*(23), 2519–2522.

Satake, K., 2002. Tsunamis, in *International Handbook of Earthquake and Engineering Seismology*, pp. 437–451, eds W.H.K. Lee, H. Kanamori, P.C. Jennings & C. Kisslinger, Academic Press, Amsterdam.

Scholz, C.H., 1982. Scaling laws for large earthquakes: consequences for physical models *Bull. Seism. Soc. Am.*, *72*, 1-14

Shapiro, N. M., Singh S. K., and Pacheco, J., 1998. A fast and simple diagnostic method for identifying tsunamigenic earthquakes, *Geophys. Res. Lett.*, 25(20), 3911-3914.

Tanioka, Y., and K. Satake, 1996. Tsunami generation by horizontal displacement of ocean bottom, *Geophys. Res. Lett.*, *23*(8), 861-864.

Tsuboi, S., K. Abe, K. Takano, and Y. Yamanaka, 1995. Rapid determination of M_w from broadband P waveforms, *Bull. Seism. Soc. Am.*, *85*, 606-613.

Tsuboi, S., P. M. Whitmore, and T. J. Sokolowski, 1999. Application of M_{wp} to deep and teleseismic earthquakes, *Bull. Seism. Soc. Am.*, *89*, 1345-1351.

Wald, D. J., V. Quitoriano, T. H. Heaton, H. Kanamori, C. W. Scrivner, and C. B. Worden, 1999. TriNet "ShakeMaps": rapid generation of instrumental ground motion and intensity maps for earthquakes in Southern California, *Earthquake Spectra*, *15*, 537–556.

Woods, M. T., and E. A. Okal, 1987. Effect of variable bathymetry on the amplitude of teleseismic tsunamis: A ray - tracing experiment, *Geophys. Res. Lett.*, *14*, 765–768.

Wu, Y-M., and H. Kanamori, 2005. Experiment on an onsite early warning method for the Taiwan early warning system, *Bull. Seism. Soc. Am.*, *95*, 347-353.

Table 1 – Assessment of tsunami potential using different discriminants

Discriminant	Available (min after OT)	Critical Value	Correctly Identified			Missed	False
			$I_t \geq 2$	%**	$I_t < 2$	$I_t \geq 2$	$I_t < 2$
M_w^{CMT}	30+	7.45	32	68%	40	15	14
M_{wp}	3-10	7.45	20	43%	45	27	9
M_{wpd} (raw)	15+	7.45	30	64%	42	17	12
T_0 (teleseismic)	15+	55	32	68%	42	15	12
L_{50}	6-10	1.0	33	70%	42	14	12
$T_d T_0$ (teleseismic)	15+	510	36	77%	47	11	7
$T_d L_{50}$	6-10	8.0	36	77%	43	11	11

* 101 events classified; 47 have $I_t \geq 2$

** percent of all events with $I_t \geq 2$ that are correctly identified

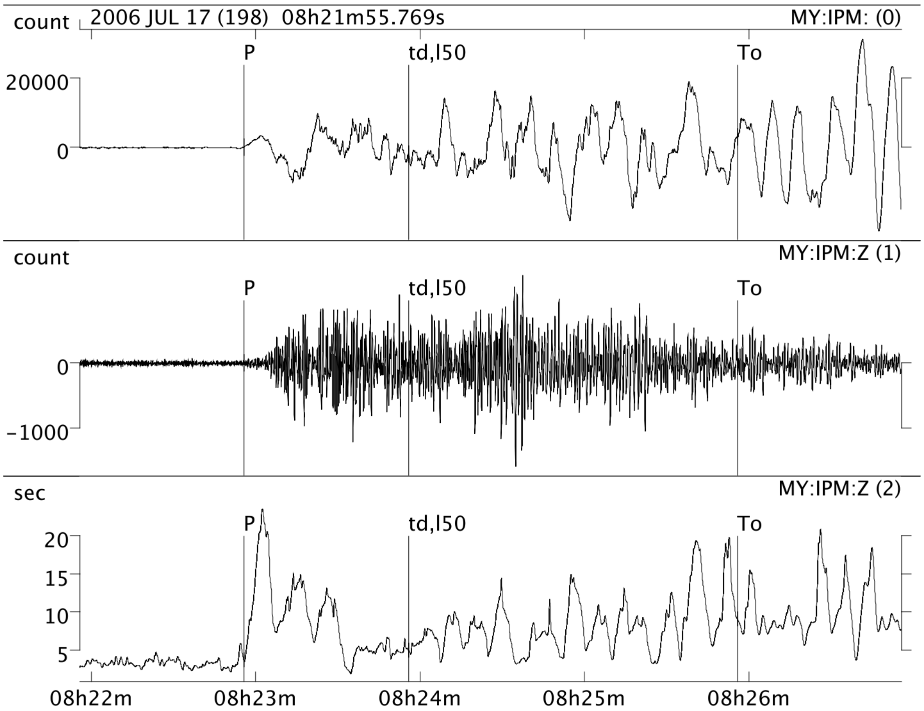

a)

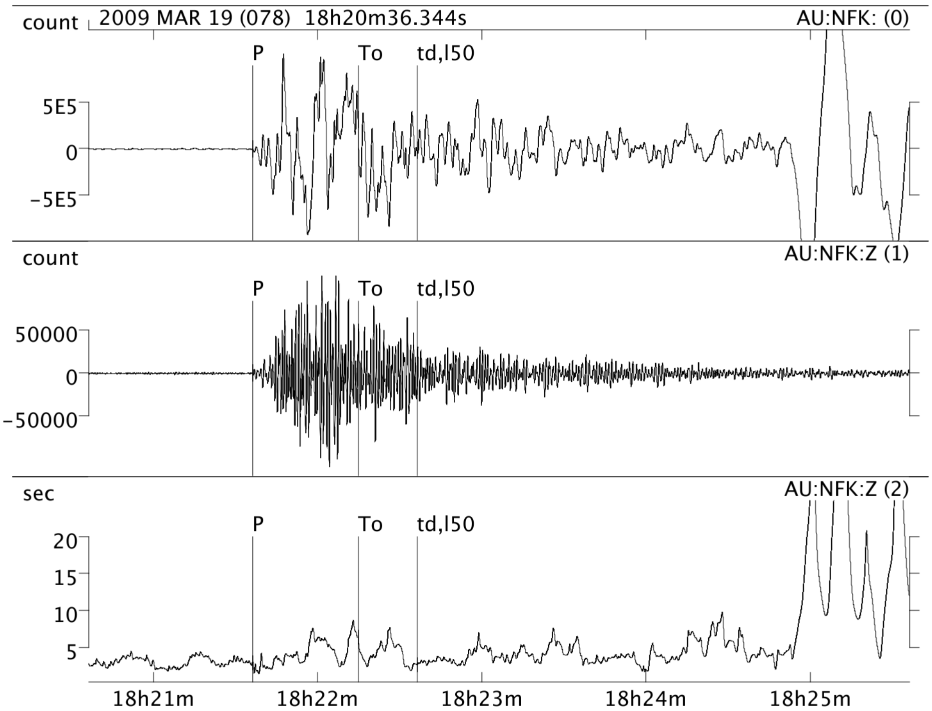

b)

Figure 1

Single-station, period-duration processing examples for (a) 2006.07.17, M_w7.7, T_0=180 s,

I_t=19, Indonesia tsunami earthquake, station MY.IPM at 15° GCD, and (b) 2009.03.19, M_w7.6, T_0=39 s, I_t=1, Tonga Islands, station AU.NFK at 17° GCD, showing raw, broadband velocity seismogram (trace 0), HF seismogram (trace 1), and T_d period (trace 2). P – automatic P pick; To – teleseismic, HF duration, T_0; td,l50 – termination time for calculation of t_d period and l_{50} DE level. Note much longer T_0 and larger t_d for the Indonesia tsunami earthquake than for the mildly tsunamigenic, Tonga Islands event of similar magnitude.

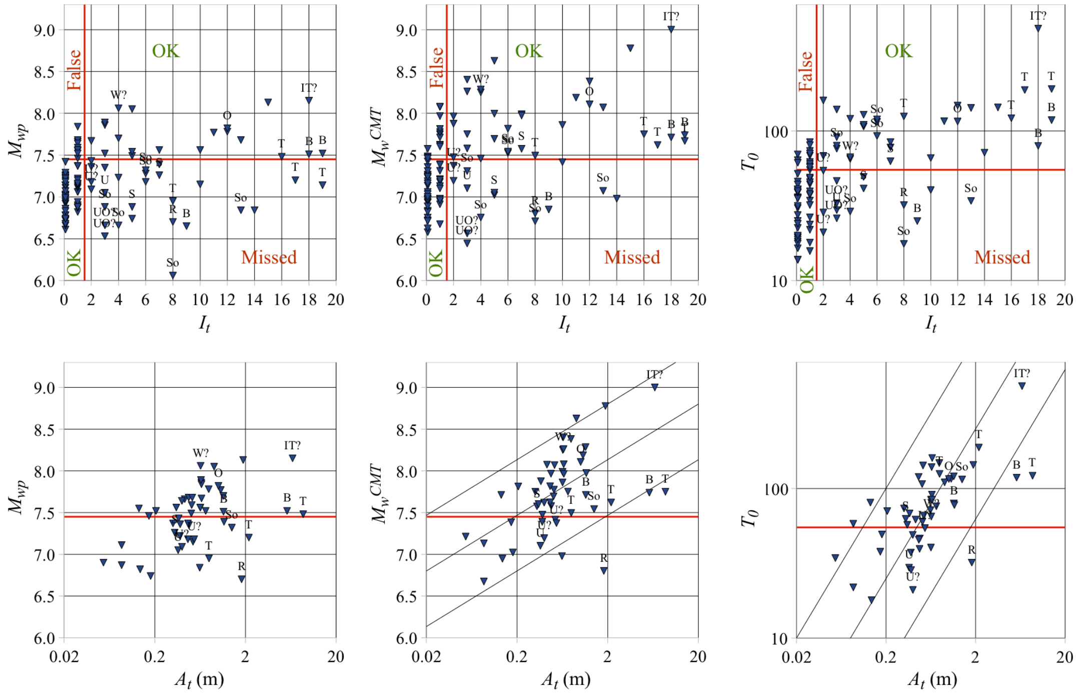

Figure 2

Comparison of body-wave moment-magnitude, M_{wp}, (left column), centroid-moment tensor magnitude, M_w^{CMT}, (centre column) and teleseismic, apparent source duration, T_0, (right column) with tsunami importance, I_t, (upper row) and representative tsunami amplitude at 100km, A_t, (lower row). Vertical red lines show the target $I_t \geq 2$ threshold; horizontal red lines show the critical values for the M_{wp}, M_w^{CMT} and T_0 discriminants (Table 1). The A_t and T_0 axes use logarithmic scaling. Parallel diagonal lines are indicative of the slope required for a linear relationships between A_t and M_0 (lower centre), A_t and T_0 (lower right). Event labels show earthquakes type for non interplate-thrust events with $I_t \geq 2$ (*I*–interplate-thrust; *T*–tsunami earthquake; O–outer-rise intraplate; B–back-arc intraplate; U-upper-plate intraplate; *So*–strike-slip oceanic, *S*–strike-slip continental, *R*–reverse-faulting).

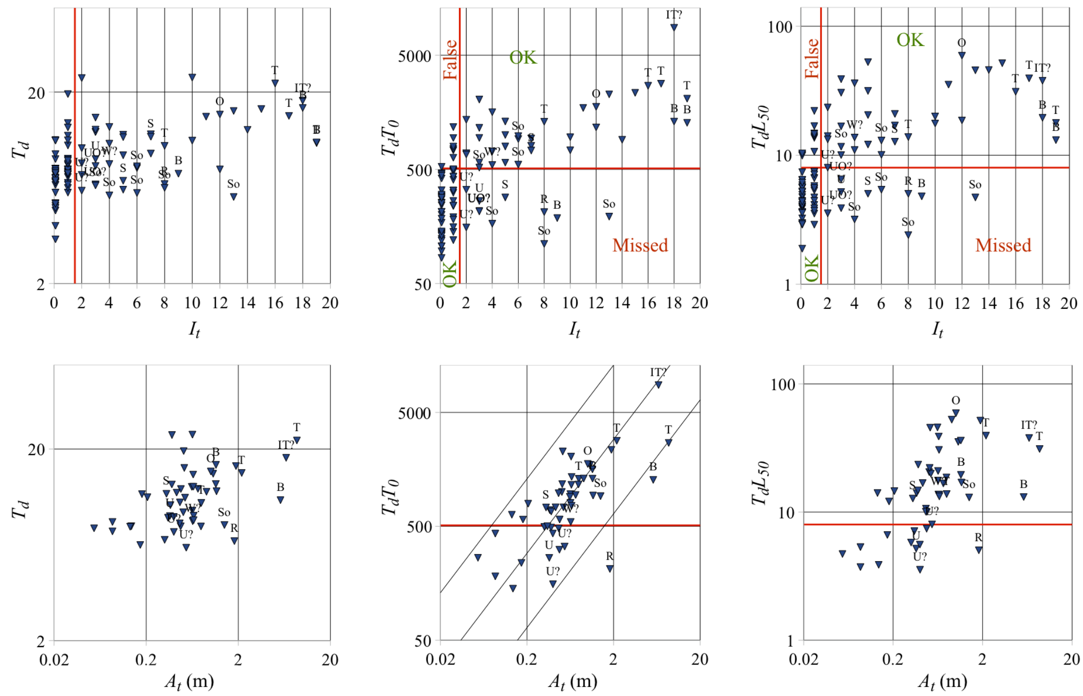

Figure 3

Comparison of dominant period, T_d, (left column), period-duration, T_dT_0, (centre column) and rapid period-duration discriminant, T_dL_{50}, (right column) with tsunami importance, I_t, (upper row) and representative tsunami amplitude at 100km, A_t, (lower row). Vertical red lines show the target $I_t \geq 2$ threshold; horizontal red lines show the critical values for the T_dT_0 and T_dL_{50} discriminants (Table 1). The A_t, T_d, T_dT_0 and T_dL_{50} axes use logarithmic scaling. Parallel diagonal lines are indicative of the slope required for a linear relationships between A_t and T_dT_0 (lower centre). Event labels as in Fig. 2.

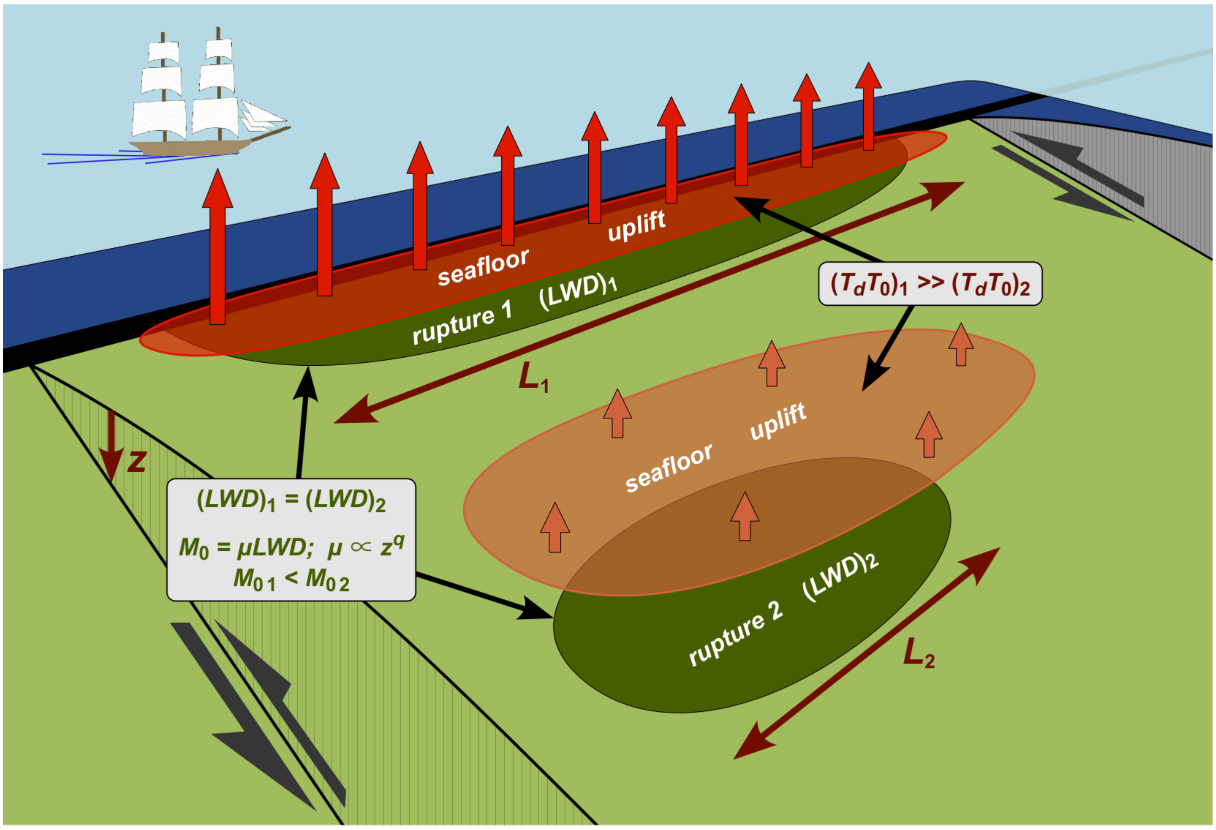

Figure 4

Simplified diagram of a subduction zone mega-thrust (pale green surface) showing two interplate thrust ruptures 1 and 2 with the same seismic potency *LWD* (dark green patches), but different vertical seafloor displacement (uplift areas shown in red and orange). The long, shallow rupture 1 produces greater total seafloor uplift than the deeper rupture 2. Since $M_0=\mu LWD$ and μ increases with depth (e.g., $\mu \propto z^q$, q positive), M_0 will be smaller for rupture 1 than for rupture 2. In contrast, since $L_1>L_2$, and v_r is lower at shallow depths, $T_0 \propto L/v_r$ will be larger for rupture 1 than for rupture 2. Since T_d may give additional information on z, W or D, the quantity $T_d T_0$ for rupture 1 can be larger or much larger than for rupture 2, correctly identifying the greater seafloor uplift and tsunami potential of the long, shallow rupture 1.